Fatigue reliability of large monopiles for offshore wind turbines

Velarde, Joey; Kramhøft, Claus; Sørensen, John Dalsgaard; Zorzi, Gianluca

Published in:
International Journal of Fatigue

DOI (link to publication from Publisher):
10.1016/j.ijfatigue.2020.105487

Publication date:
2020

Document Version
Accepted author manuscript, peer reviewed version

International Journal of Fatigue 134 (2020) 105487

Contents lists available at ScienceDirect

International Journal of Fatigue

journal homepage: www.elsevier.com/locate/ijfatigue

Fatigue reliability of large monopiles for offshore wind turbines

Joey Velarde[a,b,*], Claus Kramhøft[a], John Dalsgaard Sørensen[b], Gianluca Zorzi[c]

[a] Marine and Foundation Engineering, COWI A/S, 8000 Aarhus, Denmark
[b] Department of Civil Engineering, Aalborg University, 9100 Aalborg, Denmark
[c] GuD Geotechnik und Dynamik Consult GmbH, 10589 Berlin, Germany

ARTICLE INFO

Keywords:
Offshore wind turbines
Fatigue design
Fatigue reliability
Fatigue safety factor
Marine structures

ABSTRACT

Upscaling of traditional monopiles to support larger offshore wind turbines introduces fatigue-related design challenges. The design becomes mainly driven by wave-induced fatigue loads, and potential resonant responses can have significant contributions to fatigue. It is essential that these changes in load characteristics be reflected in the design codes. In this paper, fatigue reliability analysis of a wave sensitive, large monopile supporting a 10 MW offshore wind turbine is demonstrated. Reliability-based calibration of fatigue design factors is based on an extensive set of numerical simulations, where the statistical distribution of turbulence intensity and preservation of wave-induced resonant responses are considered. Results show that a minimum fatigue design factor, $FDF \geqslant 3$ is recommended. The results and methodology presented in this study can assist with identifying the technical limitations and economic viability of upscaling monopiles.

1. Introduction

The offshore wind industry is pushing towards development of wind turbines with higher rated capacity and installations in deeper waters. Upscaling of traditional bottom-fixed foundations, such as monopiles, introduces fatigue-related design challenges. Large monopiles become more hydrodynamically sensitive structures, and wave-induced loads and potential resonant effects can have significant contributions to fatigue. Several studies [1,2] have also shown that large monopile design is driven by fatigue limit state. Hence, the investigation of the required fatigue safety factors for large monopiles becomes important.

Current fatigue design rules are based on a semi-probabilistic approach, where partial safety factors are used to account for relevant sources of uncertainties. According to several uncertainty and sensitivity analyses [3–6] of OWT fatigue loads, uncertainties related to the fatigue damage resistance model and a few environmental parameters govern the required partial safety factors. An additional consideration for offshore wind turbine (OWT) fatigue analysis is the long-term environmental conditions, which are normally lumped into representative sea states. A lumping method that preserves wave-induced fatigue loads better than traditional methods [7,8] have been proposed in [9]. For hydrodynamically sensitive structures, it is equally important to account for uncertainties in wave load modelling [10–13]. Disregaring nonlinear wave effects can underestimate fatigue load predictions, particularly on the parked case where resonant vibrations can generate significant load amplitudes.

Compared to offshore oil & gas structures, relatively lower consequences of failure can be expected for unmanned offshore wind turbines. Applications of reliability-based methods have shown that fatigue safety factors for OWT can be reduced. Márquez-Domínguez & Sørensen [14] demonstrated the S-N approach for calibration of fatigue design factors (FDF) and investigated the effect of inspections to the required FDF values. Sørensen [15] also recommended FDF values depending on whether the structure is wind or wave dominated. Reliability-based calibration of safety factors has also been demonstrated in other structural components, such as wind turbine blades [16,17], wind turbine gearboxes [18], and deepwater risers [19].

The main objective of this work is to reassess the fatigue design factors (FDF) for a large monopile supporting a 10 MW offshore wind turbine. Reliability-based calibration of FDF is based on an extensive set of numerical simulations, where the statistical distribution of turbulence intensity and preservation of wave-induced resonant effects are considered. The recommended fatigue design factors and the sensitivity of fatigue reliability to stochastic input parameters are presented.

2. Large monopile design challenges

The primary dimensions of the monopile are designed such that the natural frequency (f_n) of the OWT is outside the blade passing frequency ranges (1P and 3P). The 1P frequency range is related to the wind

* Corresponding author.
E-mail address: jve@civil.aau.dk (J. Velarde).

https://doi.org/10.1016/j.ijfatigue.2020.105487
Received 12 July 2019; Received in revised form 6 January 2020; Accepted 16 January 2020
Available online 21 January 2020
0142-1123/

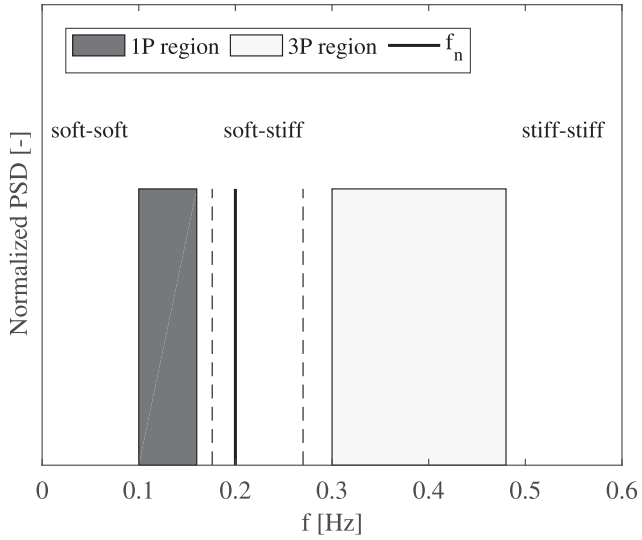

Fig. 1. DTU 10 MW reference wind turbine frequency ranges and natural frequency (f_n). The dashed lines indicate a 10% safety margin.

turbine rotor speed range (see Table 3), while the 3P frequency is related to the frequency of the three blades passing the tower. In addition, significant wave excitation frequencies are also avoided. Ideally, f_n is within the *soft-stiff* region as illustrated in Fig. 1. For larger wind turbines requiring larger bottom-fixed support structures, there is a high cost associated with increasing the overall structural stiffness. Considering a design that results to $f_n = 0.20$ Hz, the dynamic response is largely affected by wave loads, particularly during parked or standstill situations where significant aerodynamic damping is lost.

Preliminary simulations considering the parked situations are performed where fatigue loads are indicated by damage equivalent loads (*DEL*). When *DEL* is applied by an equivalent number of cycles (N_{eq}), the same amount of fatigue damage is generated as the load time history. The *DEL* for each realization are calculated using the following expression:

$$DEL = \left(\frac{\sum_{i=1}^{N_c} n_i M_i^m p}{N_{eq}} \right)^{\frac{1}{m}} \tag{1}$$

where N_c is the total number of identified cycles in the load time series, n_i is the number of load cycles corresponding to the load magnitude M_i, m is the negative inverse slope of the S-N curve (also known as the Wöhler's exponent) taken as $m = 4$, N_{eq} is the reference number of cycles taken as $N_{eq} = 2.0 \cdot 10^8$, and p is the time scale factor calculated as the ratio between the total occurrence of a sea state throughout the design life and the simulation time.

The derived normalized *DEL* isolines can be directly compared with the site-specific metocean data. Fig. 2a and b show the *DEL* isolines at the interface level and mudline level, respectively. Preliminary results indicate that for both levels, significant fatigue contributions can result from steep waves with a period (T_p) close to the first natural period ($T_n = 5$ s) of the OWT. Such dynamic effects have to be reflected in safety factors used in fatigue design of support structures. The interface level, which is defined by the connection between the wind turbine tower and the foundation, is located at 14.7 m above mean sea level (see Fig. 5).

3. Long-term environmental conditions

This section discusses the long-term environmental conditions, which served as basis for fatigue design and fatigue reliability analysis. The lumped representative sea states, where wave-induced fatigue loads are preserved, are also presented.

3.1. Metocean data

This study is based on metocean conditions for the *Vesterhav Nord* offshore wind farm (OWF), which is located at the Danish North Sea about 6 km south-west of Thyborøn. The site water depth varies from 16 m to 29 m, with a dominant wave direction approaching from north-west. The long-term metocean conditions used are based on Danish Meteorological Institute (DMI) hindcast models, which were validated against 11 years (2003–2013) of available measured data. The project site has a 50-year extreme significant wave height, $H_{ESS} = 9.0$ m and a 50-year 10-min extreme wind speed at 10 m elevation, $U_{10m} = 34.8$ m/s [20].

3.2. Wind turbulence intensity

Based on wind farm data, mean wind speed distribution at hub height and its correlation with significant wave height (H_s) are derived as shown in Fig. 3.

For fatigue analysis, the associated turbulence intensities for all wind speeds can be derived based on the *Normal Turbulence Model (NTM)* defined in the *IEC 61400-1* standard [21]. Medium turbulence characteristics (Category B) is assumed with a reference turbulence intensity, $I_{ref} = 0.14$. For a given hub height wind speed U_{hub}, the design turbulence intensity (TI_{90}) is given by the 90% quantile for turbulence standard deviation (σ_1) as defined by the Eqs. (2) and (3), respectively:

$$TI_{90} = \sigma_1 / U_{hub} \tag{2}$$

$$\sigma_1 = I_{ref}(0.75 U_{hub} + b);\ b = 5.6 m/s \tag{3}$$

For other turbulence standard deviation quantiles (σ_0), a Weibull distribution can be assumed (Eq. (4)) with scale (k) and shape (C) parameters defined by Eqs. (5) and (6), respectively.

$$F(\sigma_0 | U_{hub}) = 1 - \exp\left[-\left(\frac{\sigma_0}{C} \right)^k \right] \tag{4}$$

$$k = 0.27 U_{hub} + 1.4 \tag{5}$$

$$C = I_{ref}(0.75 U_{hub} + 3.3) \tag{6}$$

The turbulence intensity distribution at selected fractiles are summarized in Table 1, which are necessary inputs for probabilistic fatigue design or reliability-based calibration of fatigue safety factors. The characteristic value defined by the 90% percentile is used for design load calculation.

3.3. Representative sea states

Lumping of environmental conditions into scatter diagrams typically involves 12 directional sectors (30deg) for both wind and wave directions. For simplicity, the representative sea states are derived considering all directions. To preserve wave-induced responses and potential resonant effects, a finer discretization of wave peak period (T_p) close to the OWT natural period ($T_n = 5.0$ s) is considered in the scatter diagram as shown in Table 2. As oppose to using the mean T_p, the simulations are performed for different T_p considering the probability of occurrence derived from site data.

4. Foundation fatigue loads

Preliminary monopile and tower dimensions were established to support a 10 MW reference OWT [22], with key parameters summarized in Table 3. For a target natural frequency, $f_n = 0.20$ Hz, pile outer diameter at mudline level, $D_{pile} = 8.0$ m, pile thickness, $t_{pile} = 110$ mm, and pile embedment depth of 29 m are found to be feasible design assumptions. As per industry standards, the monopile diameter gradually tapers (max. 3deg) from 8.0 m to 6.5 m at the interface level. A tower

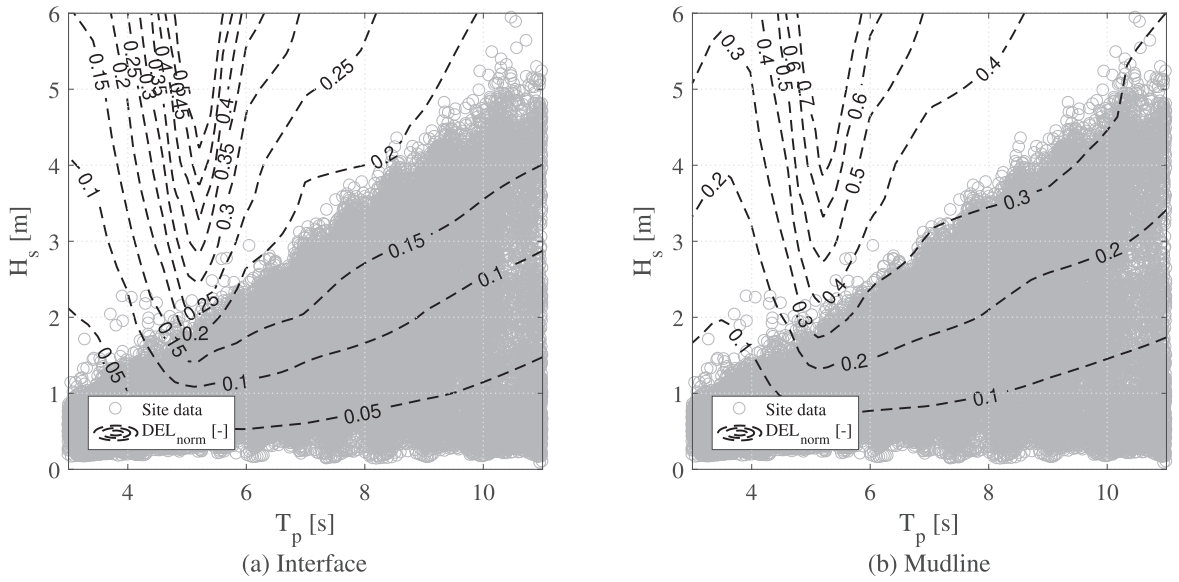

Fig. 2. Fatigue *DEL* isolines at (a) interface level and (b) mudline level during parked situations and site metocean conditions (H_s, T_p).

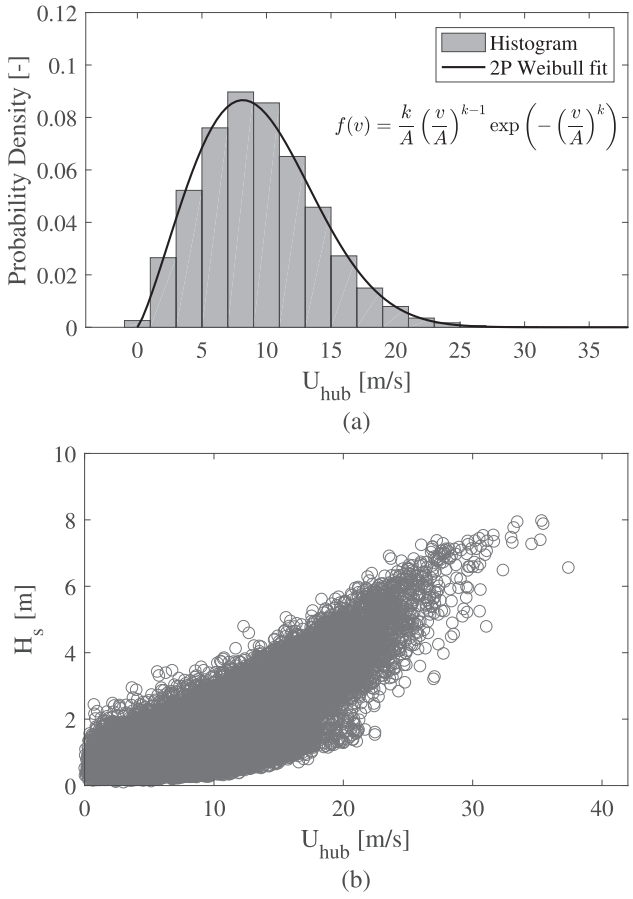

Fig. 3. Wind speed (v) distribution based on hindcast data and Weibull fit (A = 10.67 m/s, k = 2.23).

with outer diameters equal to 6.5 m at the interface level and 5.5 m at the hub elevation, supports the wind turbine at a hub height of 114 m. A fully-coupled aero-hydro-servo-elastic model is developed to perform time-domain wind turbine load simulations.

4.1. Soil-structure interaction

Typical offshore sites in the North Sea are geotechnically characterized as having fine medium sand to medium coarse sand. The assumed soil profile and soil properties summarized in Table 4 are derived from cone penetration tests (CPT) and borehole profiles typical of the North Sea. Based on the preliminary mudline load estimates and soil properties, an optimal pile embedment depth of 29 m was found based on the critical pile length criterion.

Soil-structure interaction is modelled based on the Winkler-type approach, where independent nonlinear soil springs, also referred to as p-y curves, are laterally distributed along the penetrated pile depth section. Previous studies [23–26,1] have shown that p-y curves derived based on the API method [27] tend to overestimate soil stiffness of large diameter piles, since the recommended p-y curves were initially derived for flexible piles with diameters of about 2 m. To incorporate the rigid behavior of large diameter monopiles, a geotechnical finite element code, *PLAXIS3D* [28], is used to derive the p-y curves as illustrated in Fig. 4. The *Hardening Soil model with small-strain stiffness (HSsmall)* is used to derive the p-y curves, which serve as a main input in the OWT aeroelastic model. As compared to other soil constitutive models, the *HSsmall* model can realistically capture the stiffness of the soil at low strain levels [28], which is relevant for fatigue analysis. A more detailed description of the model parameters and its derivation can be found in [29].

The monopile is modelled as a hollow steel cylinder using linear elastic plate elements, which are two-dimensional triangular elements represented by six nodes. All the sides of the model are normally fixed, and the bottom of the soil domain is fully fixed in all directions. The dimension of the soil domain in PLAXIS 3D is large enough to avoid influence on the monopile response. The 3D soil elements are modelled using tetrahedral elements with 10 nodes. Similarly, the mesh size is fine enough to have an acceptable level of accuracy.

In principle, a coupling between an aeroelastic wind turbine simulation tool and a geotechnical finite element tool can give more accurate wind turbine responses. Due to high computational effort and high number of fatigue design load cases to be evaluated, implementation of a soil finite element model is not practically done. Since monopile responses are governed by the soil lateral stiffness, representing the soil stiffness using p-y curves extracted from 3D finite element codes gives the best approximation at reasonable computational time.

Table 1
Derived turbulence intensities as a function of U_{hub} at different fractiles.

Sea state	Wind direction: 0 − 360 deg	U_{hub} [m/s]	Occ. [–]	Turbulence Intensity [-]							
				Char.	Other fractiles						
				0.90	0.05	0.20	0.35	0.50	0.65	0.80	0.95
1	4–6	5	0.053	0.262	0.067	0.114	0.145	0.173	0.201	0.235	0.294
2	6–8	7	0.104	0.217	0.069	0.108	0.132	0.153	0.174	0.198	0.239
3	8–10	9	0.152	0.192	0.072	0.106	0.126	0.142	0.158	0.177	0.208
4	10–12	11	0.179	0.176	0.075	0.104	0.121	0.135	0.149	0.164	0.189
5	12–14	13	0.171	0.165	0.077	0.104	0.118	0.130	0.142	0.155	0.176
6	14–16	15	0.130	0.157	0.079	0.103	0.116	0.127	0.137	0.148	0.166
7	16–18	17	0.092	0.151	0.081	0.103	0.115	0.124	0.133	0.143	0.159
8	18–20	19	0.055	0.146	0.082	0.103	0.114	0.122	0.130	0.139	0.153
9	20–22	21	0.030	0.142	0.083	0.103	0.113	0.121	0.128	0.136	0.148
10	22–24	23	0.016	0.139	0.085	0.103	0.112	0.119	0.126	0.133	0.145
11	24–26	25	0.007	0.136	0.086	0.103	0.111	0.118	0.124	0.131	0.141
	Total occ. [%]		**98.9**	-	12.5	15.0	15.0	15.0	15.0	15.0	12.5

4.2. Time-domain fatigue load simulations

Offshore wind turbine loads are evaluated based on simplified fatigue design load cases (DLC) defined in the IEC standards [21,30]. Fatigue time-domain simulations covering power production (*DLC*1.2) and parked cases (*DLC*6.4) are performed using the aeroelastic simulation tool *HAWC2* [31].

The DTU 10 MW reference wind turbine supported by a monopile foundation is modelled as illustrated in Fig. 5. The fully-coupled structural model is based on a multibody formulation, where each wind turbine component is represented by Timoshenko beam elements with six degrees of freedom (6 DOF), x. The general equation of motion is defined in terms of the mass matrix $[M]$, damping matrix $[D]$ and stiffness matrix $[K]$ as shown in Eq. (7).

$$[M]\ddot{x} + [D]\dot{x} + [K]x = F_{aero} + F_{hydro} \tag{7}$$

where F_{aero} and F_{hydro} are the aerodynamic and hydrodynamic forces, respectively.

The steel monopile and tower are modelled as linearly elastic bodies with Young's modulus, $E_s = 210$ GPa, and shear modulus, $G_s = 80.8$ GPa. In addition, the nacelle assembly and transition piece are represented as concentrated masses at the hub height and interface, respectively. The structural damping in *HAWC2* is formulated based on the Rayleigh viscous damping [32], where the stiffness$[K]$-proportional damping coefficient is tuned to represent the combined soil damping (D_{soil}) and structural damping (D_{struc}) contributions. Based on several OWT vibration monitoring campaigns [33,34], a damping ratio, $\zeta_{soil+struc} = 1\%$ for the first fore-aft and side-side modes is assumed. Note that the simulations also consider the aerodynamic damping (D_{aero}) and hydrodynamic damping (D_{hydro}) contributions, which are calculated based on the wind and wave input parameters and wind turbine responses. The effect of D_{aero} is primarily dependent on the blade angle of

Table 3
DTU 10 MW wind turbine main parameters and key elevations.

Parameter	Value
Rating [MW]	10
Rotor diameter [m]	178.3
Number of blades [–]	3
Cut-in, rated, cut-out U_w [m/s]	4.0, 11.4, 25.0
Rotor speed range [rpm[a]]	6, 9.6
Hub height[b] [m]	114
Interface elevation[b] [m]	14.7
Mean water depth [m]	25

[a] rpm = revolutions per minute.
[b] defined above mean sea level.

Table 4
Representative soil profile and soil properties.

	Layer	Depth [m]	E_{50}^{ref} [MPa][a]	ϕ [deg][b]
1	Fine medium sand	0 to −10	33.3	39
2	Medium coarse sand	−10 to − ∞	98.3	42

[a] E_{50}^{ref}: secant stiffness in drained triaxial test.
[b] ϕ: effective friction angle.

Table 2
Representative sea states for fatigue analysis with wave period (T_p) distribution.

Sea state	U_{hub} [m/s]	Occ. [-]	Mean H_s [m]	Mean T_p [s]	T_p [s]										
					1.5–3.5	3.5–4.5	4.5–4.7	4.7–4.9	4.9–5.1	5.1–5.3	5.3–5.5	5.5–6.5	6.5–8.5	8.5–11.5	> 11.5	Sum
					2.5	4.0	4.6	4.8	5.0	5.2	5.4	6.0	7.5	10.0	14.0	
1	5	0.053	0.82	6.8	0.0648	0.1196	0.0294	0.0390	0.0377	0.0625	0.0472	0.2812	0.1323	0.0649	0.1213	1.00
2	7	0.104	1.01	7.0	0.0124	0.0971	0.0245	0.0354	0.0307	0.0467	0.0407	0.3009	0.2537	0.0589	0.0990	1.00
3	9	0.152	1.24	7.1	0.0010	0.0330	0.0153	0.0398	0.0306	0.0515	0.0440	0.2958	0.3529	0.0777	0.0585	1.00
4	11	0.179	1.55	7.4	0.0003	0.0039	0.0026	0.0086	0.0097	0.0302	0.0336	0.3314	0.4218	0.1087	0.0492	1.00
5	13	0.171	2.01	7.8	–	–	0.0002	0.0010	0.0004	0.0024	0.0042	0.2238	0.5726	0.1564	0.0384	1.00
6	15	0.130	2.53	8.2	–	–	–	–	–	–	0.0001	0.0290	0.7136	0.2294	0.0275	1.00
7	17	0.092	3.07	8.9	–	–	–	–	–	–	–	0.0004	0.4810	0.4845	0.0341	1.00
8	19	0.055	3.65	9.9	–	–	–	–	–	–	–	–	0.0956	0.8757	0.0287	1.00
9	21	0.030	4.08	10.4	–	–	–	–	–	–	–	–	0.0054	0.9029	0.0918	1.00
10	23	0.016	4.76	11.4	–	–	–	–	–	–	–	–	–	0.6565	0.3435	1.00
11	25	0.007	5.40	12.9	–	–	–	–	–	–	–	–	–	0.2722	0.7278	1.00

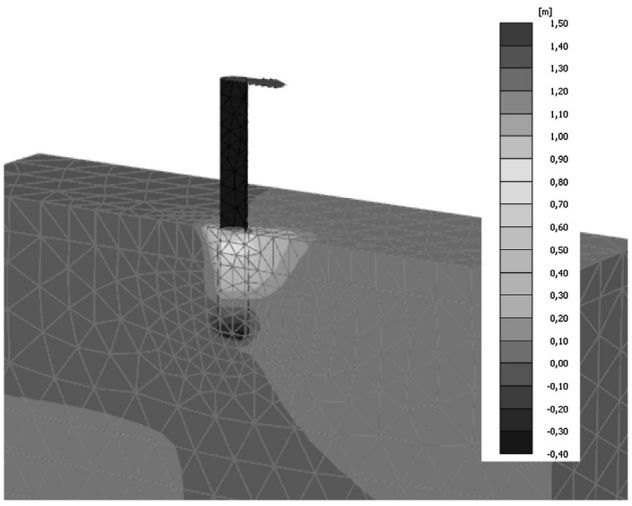

Fig. 4. Derivation of soil p-y curves in *Plaxis3D*.

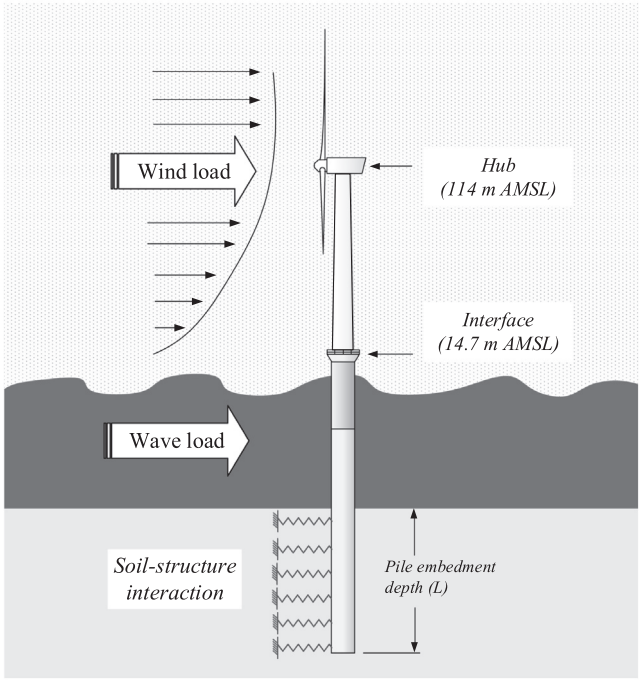

Fig. 5. Monopile-supported offshore wind turbine as modelled in HAWC2.

attack, which is a function of the incoming wind speed (U_{hub}) and wind turbine tower top motion ($\dot{u}_{top}$). Estimation and model implmentation of OWT D_{aero} can be found in several literature [7,35].

The aerodynamic loads (F_{aero}) were estimated based on the *Blade Element Momentum* (BEM) method [36,37]. Using the wind conditions presented in Section 3.2, the turbulent wind fields were generated based on the *Mann* turbulence model [38]. A power law wind profile is assumed with a mean wind shear exponent, $\alpha = 0.08$. This value is derived from wind farm design basis and is estimated by fitting the wind speed velocity profile in DMI's hindcast model for the period 2003–2013.

The hydrodynamic loads (F_{hydro}) were estimated based on Morsion's equation [39], where the total load is defined as the sum of drag and inertia components. The drag and inertia loads are function of the water density (ρ), the wave particle velocity (U) and wave particle acceleration ($\dot{U}$) as defined by Eq. (8). Drag coefficient, $C_D = 1.05$ and inertia coefficient, $C_M = 2.00$ are assumed.

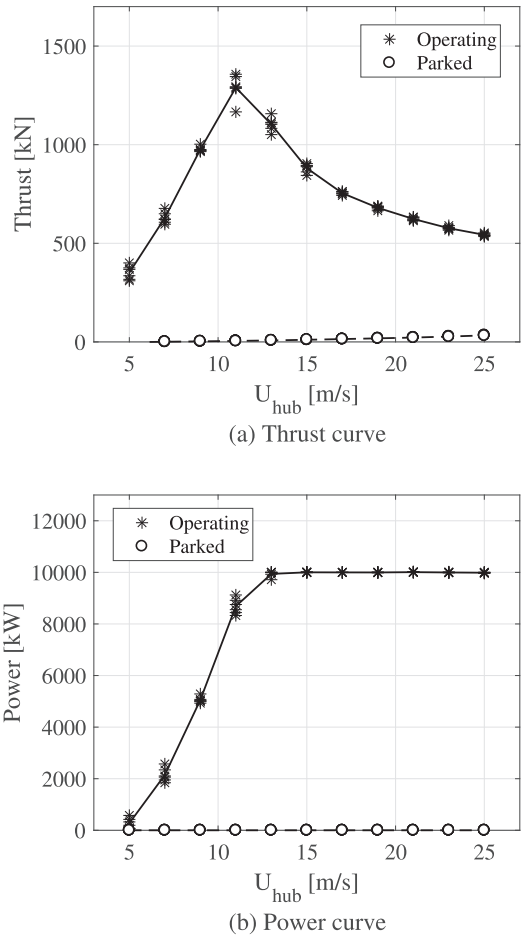

Fig. 6. DTU 10 MW Reference Wind turbine (a) thrust and (b) power curves estimated from time-domain simulations with six realizations per mean U_{hub} at TI_{90}.

$$F_{hydro} = \rho C_D D U|U| + \rho C_M A \dot{U} \tag{8}$$

For each lumped sea state presented in Section 3.3, linear irregular waves were generated based on the JONSWAP spectrum. The peak enhancement factor (γ) is determined for each sea state using the following relation [40], with H_s and T_p expressed in meters and in seconds, respectively:

$$\gamma = \begin{cases} 5, & \text{for } T_p/\sqrt{H_s} \leqslant 3.6. \\ \exp(5.75 - 1.15\frac{T_p}{\sqrt{H_s}}), & \text{for } 3.6 < T_p/\sqrt{H_s} < 5. \\ 1, & \text{for } 5 \leqslant T_p/\sqrt{H_s}. \end{cases} \tag{9}$$

The 10-min *HAWC2* simulations were performed at a timestep (Δt) of 0.02 s, with six realizations per sea state to reduce statistical uncertainties related to random realizations of the wind and wave environment. For *DLC*1.2 (power production) with 11 lumped sea states and 8 turbulence levels, a total of 528 simulations were performed. For *DLC*6.4 (parked case) where the T_p distribution is considered, 72 lumped sea states and 8 turbulence levels result to a total of 3, 456 simulations. Fig. 6 illustrates the thrust and power curves for both operating and parked situations.

The stress amplitudes and corresponding number of cycles, which are the primary load inputs for fatigue assessment, were derived from the resulting load time histories using a standard rainflow count algorithm.

5. Fatigue reliability modelling

This section presents the principles in reliability-based calibration of fatigue design factors (FDF) for OWT monopiles, as well as the underlying assumptions. A wind turbine availability of 95% (5% of the loads come from parked situation) is assumed for all calculations.

5.1. Design equation

Fatigue damage (D_f) is calculated based on S-N curve approach and linear cumulative damage theory [41,42]. The S-N relation can be written as:

$$N = K(\Delta\sigma)^{-m} \tag{10}$$

where N is the number of stress cycles to failure for a given stress range $\Delta\sigma$. K and m define the negative inverse slope and intercept, respectively, of a fatigue critical detail. Both stress concentration factor (SCF) and thickness effect are considered. Since SCF is dependent on the cross section detail and manufacturing tolerances, a value of 1.1 is assumed for welded plates with similar thickness. SCF is applied on the calculated stress time history, while the thickness effect for a plate with cross section thickness t_{cs} is accounted by modifying the nominal stress ($\Delta\sigma'$) using the reference thickness (t_{ref} = 25 mm) and thickness exponent (k = 0.10 for S-N curve $C1$) parameters as shown in Eq. (11) [43].

$$\Delta\sigma = \Delta\sigma'\left(\frac{t_{cs}}{t_{ref}}\right)^{k} \tag{11}$$

Based on the *fatigue design of offshore steel structures* standard by *Det Norske Veritas-Germanischer Lloyd* (DNVGL) [43], a bi-linear S-N curve defined by Eq. (12) is used. For structures exposed to seawater with cathodic protection, negative inverse slopes (m_1 = 3, m_2 = 5) and intercepts ($\log K_{c1}$ = 12.05, $\log K_{c2}$ = 16.08) can be assumed to calculate the characteristic S-N curve.

$$N = \begin{cases} K_{c1}\Delta\sigma^{-m_1}, & N \leqslant 10^6 \text{ cycles.} \\ K_{c2}\Delta\sigma^{-m_2}, & N > 10^6 \text{ cycles.} \end{cases} \tag{12}$$

The mean S-N curve for probabilistic analysis is calculated from the characteristic S-N curve's intercepts ($\log K_{c1}$, $\log K_{c2}$) assuming a standard deviation of 0.20 [43]. Both characteristic and mean S-N curves are illustrated in Fig. 7.

The design equation for fatigue limit state is formulated as shown in Eq. (13), with stresses calculated from simulations using characteristic turbulence level, $TI_{0.90}$. The occurrence probability (p_i) of fatigue sea state i is related to the discretized wind (U_{hub}) and wave (H_s, T_p) distribution. For this exercise, the pile thickness (t_{pile}) is selected as the design parameter ($\mathbf{z}$) with the pile diameter assumed constant (D_{pile} = 8.0 m).

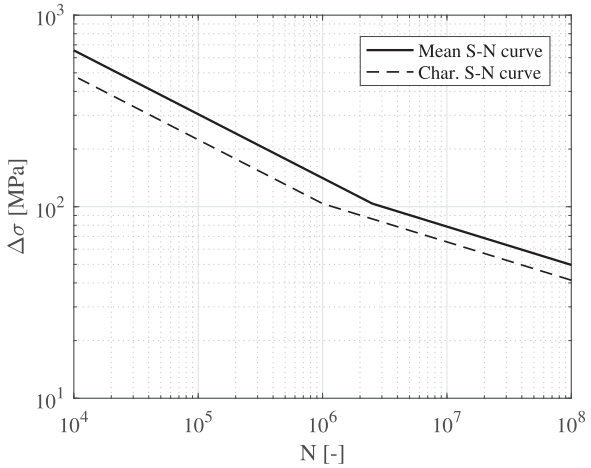

Fig. 7. Bi-linear S-N curve for seawater environment with cathodic protection. Curve C_1 is assumed for welds ground flushed to the plate surface.

$$G(\mathbf{z}) = 1 - \sum_{i=U_{in}}^{U_f}\sum_{j=\Delta\sigma_1}^{\Delta\sigma_{cut}} \frac{n_{i,j,k}p_i FDFT_L}{K_{c1}\Delta\sigma_{i,j,k}^{-m_1}} - \sum_{i=U_{in}}^{U_f}\sum_{j=\Delta\sigma_{cut}}^{\Delta\sigma_\infty} \frac{n_{i,j,k}p_i FDFT_L}{K_{c2}\Delta\sigma_{i,j,k}^{-m_2}} = 0 \tag{13}$$

where:

U_{in}, U_{out} are the cut-in and cut-out wind speeds, respectively
$\Delta\sigma_1$, $\Delta\sigma_\infty$ are the initial and final stress range bins, respectively
$\Delta\sigma_{cut}$ is the stress range bin at the intersection of the bi-linear S-N curves
$n_{i,j}$ is the number of stress cycles per year at bin i, j
$\Delta\sigma_{i,j}$ is the stress range at bin i, j
T_L is the design lifetime (25 years)

5.2. Limit state equation

The limit state equation is formulated as shown in Eq. (14). The probability ($p_{i,j}$) represents the occurrence fatigue sea state i for each turbulence intensity fractile j.

$$\begin{aligned} g(\mathbf{z}, t) &= \Delta - \sum_{i=U_{in}}^{U_{out}}\sum_{j=TI_{0.05}}^{TI_{0.95}}\sum_{k=\Delta\sigma_1}^{\Delta\sigma_{cut}} \frac{n_{i,j,k}p_{i,j}t}{K_1\Delta\sigma_{i,j,k}^{-m_1}}(X_{SCF}X_{dyn}X_{wave})^{m_1} - \\ &\sum_{i=U_{in}}^{U_{out}}\sum_{j=TI_{0.05}}^{TI_{0.95}}\sum_{k=\Delta\sigma_{cut}}^{\Delta\sigma_\infty} \frac{n_{i,j,k}p_{i,j}t}{K_2\Delta\sigma_{i,j,k}^{-m_2}}(X_{SCF}X_{dyn}X_{wave})^{m_2} \end{aligned} \tag{14}$$

where:

Δ is the Miner's rule model uncertainty related to linear damage accummulation
$p_{i,j}$ is the occurrence probability of sea state i, j
t is the time in years ($0 \leqslant t \leqslant T_L$)
K_1 and K_2 are related to the mean intercepts, $\log K_1$ and $\log K_2$
X_{SCF} is the SCF model uncertainty
X_{dyn} is the dynamic model uncertainty
X_{wave} is the wave load model uncertainty

The list of deterministic and stochastic variables are summarized in Table 5, with X_{dyn} evaluated at different uncertainty levels. The probability of failure at time t, $P_F(\mathbf{z}, t) = P(g(\mathbf{z}, t) \leqslant 0)$, is evaluated based on Eq. (14) using First Order Reliability Method (FORM) [44]. Consequently, the corresponding reliability index is estimated as $\beta(\mathbf{z}, t) = -\Phi^{-1}(P_F(\mathbf{z}, t))$, where Φ is the standard normal distribution function. For a reference period of one year, the annual probability of failure (ΔP_F) and annual reliability index ($\Delta\beta$) can be obtained by Eqs. (15) and (16), respectively.

Table 5
Stochastic model for the welded steel detail. N: Normal; D: Deterministic; LN: LogNormal.

Variable	Dist.	Mean	COV	Std. dev.	Ref.
Δ	N	1.00	0.30	–	[45]
$\log K_1$	N	12.45	–	0.20	[43]
$\log K_2$	N	16.48	–	0.20	[43]
m_1	D	3	–	–	[43]
m_2	D	5	–	–	[43]
X_{SCF}	LN	1.00	0.05	–	[15]
X_{dyn}	LN	1.00	0, 0.05, **0.10**, 0.15	–	[5,46],[a]
X_{wave}	LN	1.00	0.10	–	[15,47]

[a] Expert opinion.

$$\Delta P_F(\mathbf{z}, t) = \frac{P_F(\mathbf{z}, t + \Delta t) - P_F(\mathbf{z}, t)}{(1 - P_F(\mathbf{z}, t))\Delta t} \quad (15)$$

$$\Delta\beta(\mathbf{z}, t) = -\Phi^{-1}(\Delta P_F(\mathbf{z}, t)) \quad (16)$$

where $t > \Delta t$ and Δt is the time interval in years.

5.3. Safety factor calibration

Being unmanned structures, offshore wind turbines are classified as having minor consequences of failure with large relative cost of safety measure [48]. This corresponds to a target annual reliability index of $\Delta\beta = 3.1 (P_F \approx 10^{-3})$, which serves as primary basis for reliability-based calibration of safety factors in recognized design codes. The procedure for calibration of fatigue design factors (FDF) is outlined as follows:

1. Choose a design parameter, $\mathbf{z} = t_{pile}$ (pile thickness). This parameter is normally expressed in terms of the ratio between pile diameter and pile thickness ($D_{pile}/t_{pile}ratio$).
2. For selected FDF values, calculate resulting t_{pile} such that the design Eq. (13) is equal to zero. By redoing the calculation for several FDF values, a relation between FDF and $D_{pile}/t_{pile}ratio$ can be found as shown in Fig. 8.
3. Consider FDF = [1–3,5,10] with corresponding t_{pile} summarized in Table 6. Current manufacturing technology is limited to about $t_{pile} = 120$ mm ($D_{pile}/t_{pile} \approx 67$).
4. Perform reliability analysis for selected FDF values and corresponding $\mathbf{z} = t_{pile}$ using the limit state Eq. (14).

The presence of marine growth can affect design load calculations for offshore wind turbines [49,50]. But this does not affect the recommended partial safety factors, because the effect of incorporating the marine growth in the load model cancels out in the design load model and the probabilistic load model.

6. Results and discussion

The fatigue design calculations and probabilisitc fatigue analysis are presented in this section. The last subsection recommends fatigue design factors for design of large OWT monopiles, and also investigates the sensitivity of fatigue reliability to stochastic input parameters.

6.1. Fatigue design loads

The fatigue design loads were calculated from the design equation, where characteristic S-N curve and characteristic turbulence intensity ($TI_{90\%}$) were applied. The calculated 25-year fatigue damage (D_f) at mudline level is summarized in Table 7, assuming a 95% wind turbine availability. The D_f distribution across mean wind speeds at hub height is illustrated in Fig. 9. Despite having a 5% occurrence, the parked or standstill case has a 45% relative contribution to the total D_f.

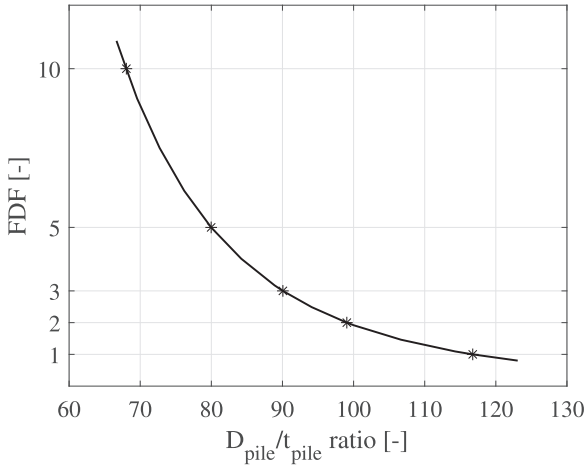

Fig. 8. FDF as a function of pile D/t ratio (pile D = 8.0 m).

Table 6
Estimated pile thickness at mudline for selected FDF.

FDF [–]	$D_{pile}/t_{pile}ratio$ [–]	t_{pile} [mm]
1	117	69
2	99	81
3	90	89
5	80	100
10	68	118

Table 7
Calculated 25-year fatigue damage (D_f) at mudline assuming 95% wind turbine availability (Pile $D/t = 73$).

Sea state	U_w [m/s]	Operation	Standstill	Total
1	5	0.0001	0.0001	0.0002
2	7	0.0005	0.0003	0.0008
3	9	0.0029	0.0014	0.0043
4	11	0.0073	0.0047	0.0120
5	13	0.0113	0.0119	0.0232
6	15	0.0110	0.0151	0.0262
7	17	0.0112	0.0104	0.0217
8	19	0.0104	0.0069	0.0173
9	21	0.0083	0.0060	0.0142
10	23	0.0062	0.0028	0.0090
11	25	0.0033	0.0011	0.0044
TOTAL		0.073	0.061	**0.133**

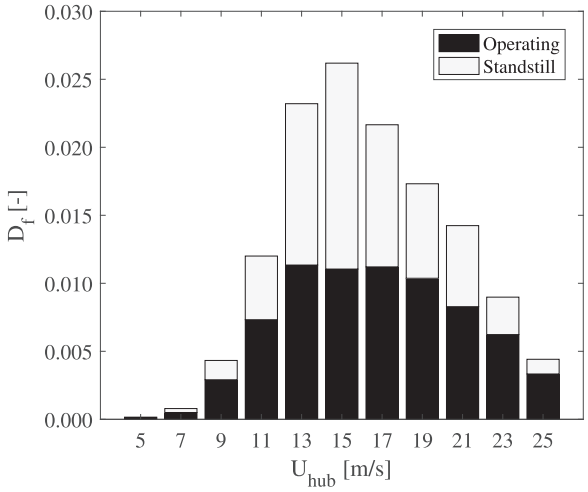

Fig. 9. Fatigue damage (D_f) distribution across different sea states assuming 95% wind turbine availability.

Although a major interest in OWT fatigue analysis is the relative contributions of wind and wave-induced fatigue loads, evaluation using integrated OWT models is not direct forward. Performing time-domain simulations without the turbulent wind fields disregards the aerodynamic damping, which leads to significant overestimation of the wave-induced loads. An alternative procedure for estimation of wave load contribution is to include the wind fields with constant wind speed (without turbulence). Thereafter, the wind load contribution can be estimated as the difference between the initial fatigue damage and the wave load contribution. The same approach is applied for the calculated design loads as illustrated in Fig. 10. Considering the power production case (100% availability) results to 22.60% wave-induced D_f, while assuming a 95% availability increases the wave contribution

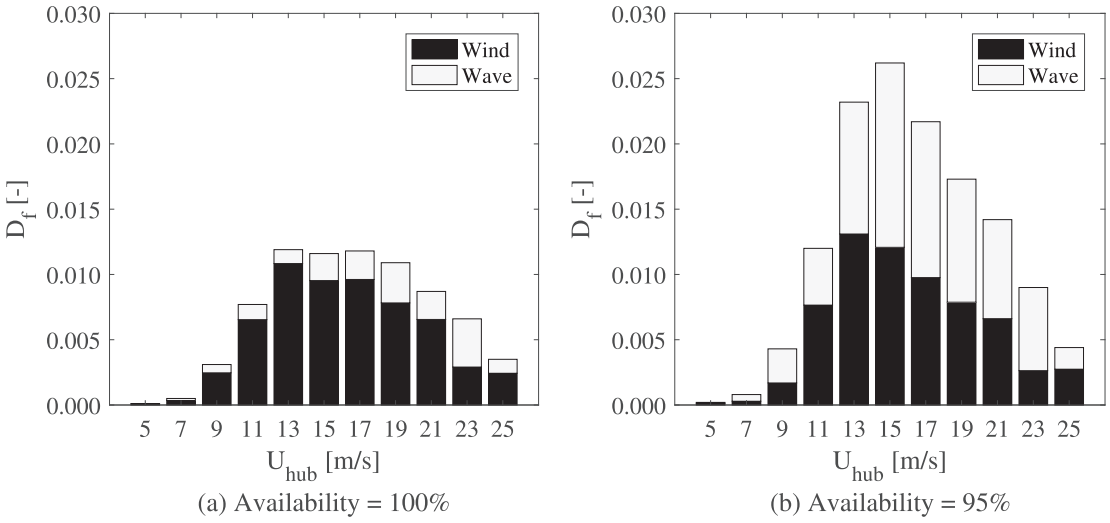

Fig. 10. Relative wind and wave contribution to total fatigue damage (D_f).

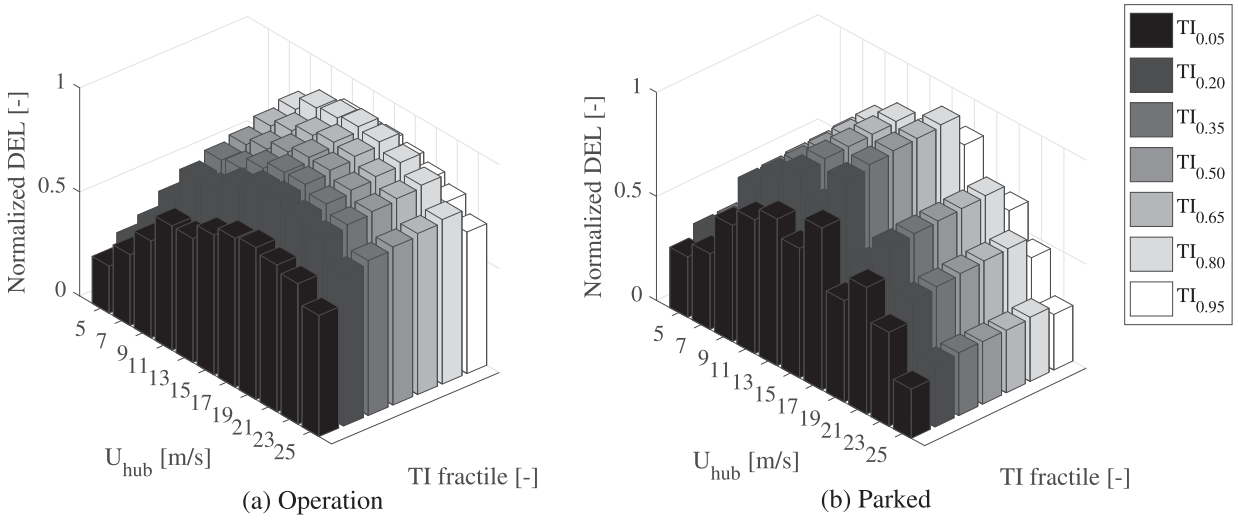

Fig. 11. Normalized fatigue damage equivalent load (*DEL*) for different wind speeds (U_{hub}) and turbulence intensity (*TI*) fractiles. Both U_w and *TI* occurrence probabilities are included.

Table 8
Annual reliability index ($\Delta\beta$) at $T_L = 25 years$.

X_{dynCOV}	FDF				
	1	2	3	5	10
0.00	2.46	3.01	3.38	3.87	4.22
0.05	2.44	2.96	3.27	3.82	4.22
0.10	**2.40**	**2.84**	**3.13**	**3.53**	**4.19**
0.15	2.37	2.73	2.95	3.26	4.12

to about 51.6%. This indicates that the large monopile design leads to a wave-sensitive structure, particularly during parked situations.

Estimation of design loads for OWT support structures incorporates safety margins when considering the 90% quantile for turbulence intensity. This safety margin is reduced as the relative contribution of wave-induced loads increases. These changes in load characteristics, which are related to upscaling monopiles, have to be reflected in fatigue design factors.

6.2. Fatigue load distribution for probabilistic analysis

For probabilistic analysis, the turbulence intensity distribution is

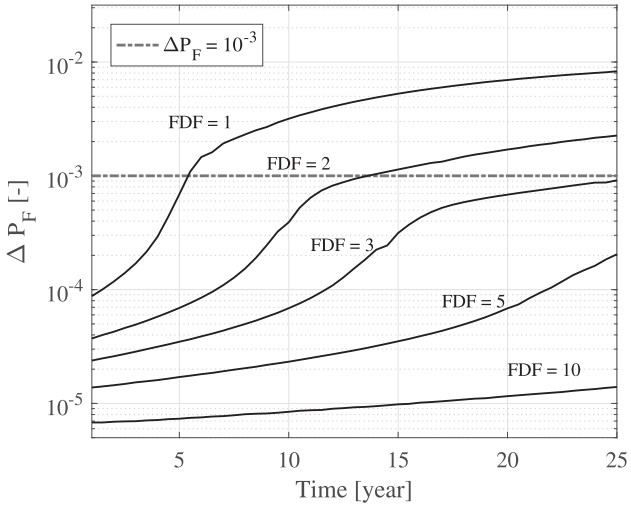

Fig. 12. Time-dependence of annual probability of failure (ΔP_F) for different FDF values ($X_{dynCOV} = 0.10$).

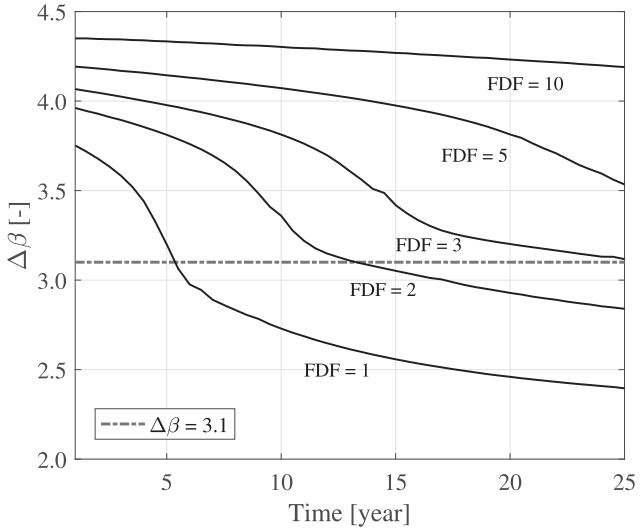

Fig. 13. Time-dependence of annual reliability index ($\Delta\beta$) for different FDF values (X_{dynCOV} = 0.10).

Table 9
Calculated sensitivity factors (α_i) and design points (X_i) at FDF = 3 (X_{dynCOV} = 0.10), t = 3 & 25 years.

Parameter	t = 3 year		t = 25 year	
	α_i	X_i	α_i	X_i
Δ	0.9991	0.01	0.4837	0.65
X_{SCF}	−0.0120	1.00	−0.2495	1.03
X_{dyn}	−0.0249	1.00	−0.5173	1.13
X_{wave}	−0.0249	1.00	−0.5173	1.13
logK_1	0.0006	12.45	0.0052	12.45
logK_2	0.0196	16.47	0.4106	16.28

directly considered in the OWT fatigue design load calculation. Fig. 11 illustrates the distribution of the normalized fatigue damage equivalent load (*DEL*) as a function of U_{hub} and turbulence intensity (*TI*). As expected, higher *TI* results to higher *DEL* during power production. In contrast, there is no significant difference observed during parked situations.

6.3. Fatigue reliability and recommended safety factors

The reliability against fatigue failure is evaluated based on the limit state equation (Eq. (14)) and the stochastic material model with parameters summarized in Table 5. The same procedure is performed for different FDF values with corresponding design parameter t_{pile}. For simplicity, it is assumed that the calculated loads for pile D/t = 73 (t_{pile} = 110 mm) are applicable for all pile D/t ratios considered. Changes in the overall natural frequency and ULS utilization factor are not investigated.

The predicted fatigue annual reliability indices ($\Delta\beta$) for different FDF values are summarized in Table 8, which also shows the sensitivity to the dynamic model uncertainty (X_{dyn}). Assuming a X_{dynCOV} = 0.10, a $FDF \geqslant 3$with $\Delta\beta \geqslant 3.1 (P_F \approx 10^{-3})$ is recommended for large monopiles. This is in general agreement with DNVGL standard for *Support structures for wind turbines* [51], which requires a minimum FDF = 3 for failure-critical sections not accessible for inspections or repairs.

The time-dependence of annual probability of failure (ΔP_F) and annual reliability index ($\Delta\beta$) are illustrated in Figs. 12 and 13, respectively. The behaviour of the curves indicates that at the beginning of lifetime, the uncertainty is governed by the Miner's rule uncertainty, Δ. Whereas towards the end of the lifetime, load-related uncertainties are observed to have significant contributions to the total uncertainties. These results can be extended by including reliability updating based on inspections and by performing risk-based inspection planning.

The sensitivity of $\Delta\beta$ to stochastic input parameters and the estimated design points are summarized in Table 9 for t = 3 years and t = 25 years. Based on the α_i^2 values, the relative importance of the stochastic input parameters can be illustrated as shown in Fig. 14. The small sensitivity to S-N curve parameter, logK_1, implies that a significant part of the fatigue stress ranges are small amplitude cycles that are covered by the S-N slope, m_2 = 5. For this case study, the stochastic parameters Δ, logK_2, X_{dyn} and X_{wave} govern the uncertainties in fatigue reliability.

7. Conclusions

This study demonstrated fatigue reliability analysis of a wave sensitive, large monopile supporting a 10 MW offshore wind turbine. Considering the relevant sources of uncertainties, a minimum fatigue design factor ($FDF \geqslant 3$) is recommended. The sensitivity of fatigue reliability to stochastic input parameters was also quantified.

A number of assumptions that can affect the results have been made to simplify the analysis. The effects of nonlinear wave modelling, wind-wave misalignment, wind farm wakes and fatigue inspections were not considered in this study. The sensitivity with respect to the choice of S-N curves was also disregarded.

Finally, the results can vary depending on wind turbine size and site-specific metocean conditions. Designing monopiles for larger wind turbines or at higher water depths increases the relative contribution of wave-induced fatigue loads, which reduces the safety margin from

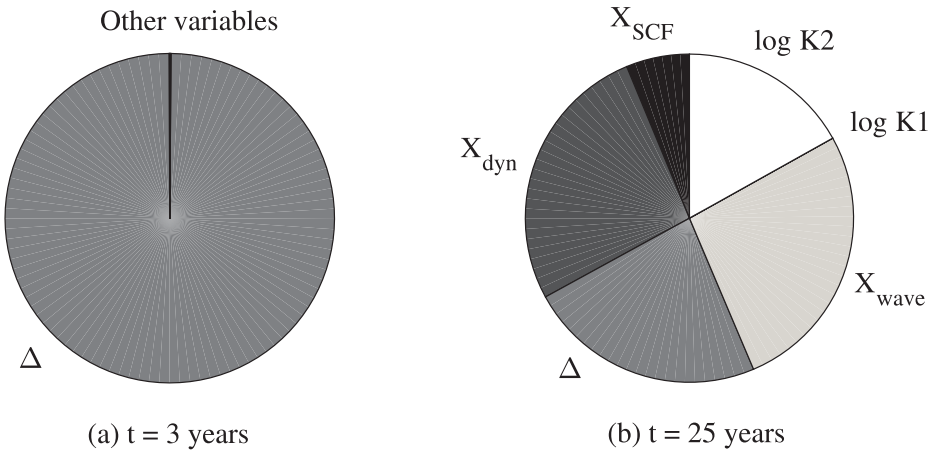

Fig. 14. Sensitivity (α_i^2) of $\Delta\beta$ to stochastic input parameter evaluated for FDF = 3 (X_{dynCOV} = 0.10) at (a) t = 3 years & (b) t = 25 years.

designing against the 90% turbulence intensity quantile. Consequently, a higher FDF value will be required for such cases. The results and methodology presented in this study can assist with identifying the technical limitations and economic viability of upscaling monopiles.

Declaration of Competing Interest

None.

Acknowledgements

This research work was performed within the European project INFRASTAR, which has received funding from the European Union's Horizon 2020 research and innovation programme under the Marie Skłodowska-Curie grant agreement No. 676139.

References

[1] Velarde Joey, Bachynski Erin E. Design and fatigue analysis of monopile foundations to support the DTU 10 MW offshore wind turbine. Energy Proc 2017;137:3–13.
[2] Njomo Wandji Wilfried, Natarajan Anand, Krasimirov Dimitrov Nikolay. Influence of model parameters on the design of large diameter monopiles for multi-megawatt offshore wind turbines at 50-m water depths. Wind Energy 2017.
[3] Veldkamp Dick. A probabilistic evaluation of wind turbine fatigue design rules. Wind Energy 2008;11(6):655–72.
[4] Hubler Clemens, Gebhardt Cristian Guillermo, Rolfes Raimund. Hierarchical four-step global sensitivity analysis of offshore wind turbines based on aeroelastic time domain simulations. Renew Energy 2017;111:878–91.
[5] Velarde Joey, Kramhøft Claus, Sørensen John Dalsgaard. Global sensitivity analysis of offshore wind turbine foundation fatigue loads. Renew Energy 2019. https://doi.org/10.1016/j.renene.2019.03.055. ISSN: 0960-1481. http://www.sciencedirect.com/science/article/pii/S096014811930360X.
[6] Velarde Joey, et al. Uncertainty modeling and fatigue reliability assessment of offshore wind turbine concrete structures. Int J Offshore Polar Eng 2019;29(02):165–71.
[7] Johannes Kuhn Martin. Dynamics and design optimisation of offshore wind energy conversion systems. DUWIND: Delft University Wind Energy Research Institute; 2001.
[8] Fischer T, De Vries WE, Schmidt B. UpWind Design Basis (WP4: Offshore foundations and support structures); 2010.
[9] Passon Patrik, Branner Kim. Condensation of long-term wave climates for the fatigue design of hydrodynam-ically sensitive offshore wind turbine support structures. Ships Offshore Struct 2016;11(2):142–66.
[10] Passon Patrik. Damage equivalent wind-wave correlations on basis of damage contour lines for the fatigue design of offshore wind turbines. Renew Energy 2015;81:723–36.
[11] Seidel Marc, Voormeeren Sven, van der Steen Jan-Bart. State-of-the-art design processes for offshore wind turbine support structures. Stahlbau 2016;85(9):583–90.
[12] Marino Enzo, Giusti Alessandro, Manuel Lance. Offshore wind turbine fatigue loads: the influence of alternative wave modeling for different turbulent and mean winds. Renew Energy 2017;102:157–69.
[13] Colone Lorenzo, Natarajan Anand, Dimitrov Nikolay. Impact of turbulence induced loads and wave kinematic models on fatigue reliability estimates of offshore wind turbine monopiles. Ocean Eng 2018;155:295–309.
[14] Marquez-Dominguez Sergio, Sørensen John D. Fatigue reliability and calibration of fatigue design factors for offshore wind turbines. Energies 2012;5(6):1816–34.
[15] Sørensen Dalsgaard John, et al. Reliability-based calibration of fatigue safety factors for offshore wind turbines. Int J Offshore Polar Eng 2012;22(03).
[16] Ronold Knut O, Wedel-Heinen Jakob, Christensen Carl J. Reliability-based fatigue design of wind-turbine rotor blades. Eng Struct 1999;21(12):1101–14.
[17] Stensgaard Toft Henrik, Sørensen John Dalsgaard. Reliability-based design of wind turbine blades. Struct Saf 2011;33(6):333–42.
[18] Nejad Amir Rasekhi, Gao Zhen, Moan Torgeir. On long-term fatigue damage and reliability analysis of gears under wind loads in offshore wind turbine drivetrains. Int J Fatigue 2014;61:116–28.
[19] Leira Bernt J, et al. Assessment of fatigue safety factors for deep-water risers in relation to VIV. J Offshore Mech Arctic Eng 2005;127 A:353–8.
[20] Nord Vesterhav. Offshore wind farm metocean report. Tech. rep. COWI A/S; 2015.
[21] International Electrotechnical Commission et al. IEC 61400–1. In: Wind Turbines—Part 1: Design Requirements f; 2019.
[22] Christian Bak et al. Description of the DTU 10 MW reference wind turbine. In: DTU Wind Energy Report-I-0092 5 (2013).
[23] Lesny K, Wiemann J. Finite-element-modelling of large diameter monopiles for offshore wind energy converters. In: GeoCongress 2006: geotechnical engineering in the information technology age; 2006. p. 1–6.
[24] Augustesen Anders Hust et al. Numerical modelling of large-diameter steel piles at Horns Rev.; 2009.
[25] Zdravkovic L, et al. Numerical modelling of large diameter piles under lateral loading for offshore wind applications. Front Offshore Geotech III 2015:759–64.
[26] Byrne BW et al. PISA: new design methods for offshore wind turbine monopiles; 2017.
[27] American Petroleum Institute. Recommended practice for planning, designing, and constructing fixed offshore platforms. Vol. 2. American Petroleum Institute; 1989.
[28] BV Plaxis. Plaxis material models manual. In: The Netherlands; 2019.
[29] Zorzi Gianluca, et al. Reliability analysis of offshore wind turbine foundations under lateral cyclic loading English. Wind Energy Sci. 2019. ISSN: 2366-7443.
[30] International Electrotechnical Commission et al. IEC 61400–3. In: Wind Turbines—Part 3: Design Requirements for Offshore Wind Turbines; 2009.
[31] Larsen Torben Juul, Hansen Anders Melchior. How 2 HAWC2, the user's manual. In: target 2; 2015, p. 2.
[32] Rayleigh Lord. Theory of sound (two volumes). New York: Dover Publications; 1897.
[33] Devriendt Christof, et al. Damping estimation of an offshore wind turbine on a monopile foundation. IET Renew Power Gener 2013;7 A:40112.
[34] Shirzadeh Rasoul, et al. The dynamics of an offshore wind turbine in parked conditions: a comparison between simulations and measurements. Wind Energy 2015;18(10):1685–702.
[35] Van Der Tempel Jan. Design of support structures for offshore wind turbines; 2006.
[36] Glauert Hermann. Airplane propellers. Aerodynamic theory. Springer; 1935. p. 169–360.
[37] Hansen Martin OL, Madsen Helge Aagaard. Review paper on wind turbine aerodynamics. J Fluids Eng 2011;133(11):114001.
[38] Mann Jakob. Wind field simulation. Probabil Eng Mech 1998;13(4):269–82.
[39] Morison JR, Johnson JW, Schaaf SA, et al. The force exerted by surface waves on piles. J Petrol Technol 1950;2(05):149–54.
[40] GL DNV. Environmental conditions and environmental loads. In: Recommend Practice DNV-RP-C205; 2017.
[41] Palmgren Arvid. Die lebensdauer von kugellagern. Zeitschrift des Vereins Deutscher Ingenieure 1924;68(14):339–41.
[42] Miner Milton A, et al. Cumulative damage in fatigue. J Appl Mech 1945;12(3):159–64.
[43] GL DNV. Fatigue design of offshore steel structures. In: Standard DNVGL-ST-C203 20; 2016.
[44] Madsen Henrik O, Krenk Steen, Lind Niels Christian. Methods of structural safety. Courier Corporation; 2006.
[45] Folsø Rasmus, Otto Sven, Parmentier Guy. Reliability-based calibration of fatigue design guidelines for ship structures. Mar Struct 2002;15(6):627–51.
[46] JD S0rensen and HS Toft. Safety Factors—IEC 61400-; 4—Background Document. In: DTU Wind Energy-E-Report-0066 (EN); 2014.
[47] JCSS JCSS. Probabilistic model code. In: Joint Committee on Structural Safety; 2001.
[48] International Standards Organization. ISO 2394: 2015: general principles on reliability for structures; 2015.
[49] Ameryoun Hamed, et al. Stochastic modeling of forces on jacket-type offshore structures colonized by marine growth. J Mar Sci Eng 2019;7(5):158.
[50] Spraul Charles et al. Effect of marine growth on floating wind turbines mooring lines responses. In: Congres francais de mecanique. AFM, Association Frangaise de Mecanique; 2017.
[51] GL DNV. Support structures for wind turbines. In: Standard DNVGL-ST-0126; 2018.